Cellular and Molecular Life Sciences (2025) 82:106
https://doi.org/10.1007/s00018-025-05597-w

ORIGINAL ARTICLE

Unveiling two distinct osteolineage cell populations linked to age-related osteoporosis in adult mice through integrative single-cell analyses

Bo Zhou[1] · Hongwen Huang[2] · Zhen Ding[1] · Kaiwen Luo[2] · Yangshan Chen[1] · Yingying Han[1] · Wei Pang[1] · Wanze Tang[1] · Litong Chen[1] · Wenfei Jin[3] · Guixing Ma[1] · Huiling Cao[1]

Received: 24 June 2024 / Revised: 13 January 2025 / Accepted: 15 January 2025

Abstract

The bone marrow microenvironment contains heterogeneous stromal cells, which are critical for bone remodeling and provide essential supportive roles for hematopoietic functions. Although the diversity of PDGFRα^{+}β^{+} mesenchymal stromal/stem cells (MSCs) get consensus, the osteo-lineage cells (OLCs) that constitute the developmental trajectory of osteoblasts are largely remain unclear. Here, we construct a comprehensive atlas of stromal cell via performing integrative single cell analyses for 77 samples from 14 datasets. Besides previously defined Lepr^{+} BM-MSCs derived OLC1, we present a novel OLC2 with unique molecular signatures and differentiation pathway. Both OLC1 and OLC2 show significant polygenic association with bone mineral density (BMD), while extracellular matrix (ECM) proteins specifically expressed by OLC2 are particularly decreased in bone tissue of aged mice. Notably, OLC1 and OLC2 are consistently reduced in aged mice, which might be induced by the decreased expression of several lineage drivers. Collectively, our study presents a thorough prospect of OLCs in the bone marrow microenvironment and highlights their important roles in age-related osteoporosis.

Keywords Bone marrow microenvironment · Bone remodeling · MSC · Osteo-lineage cell · Osteoporosis

Introduction

Bone undergoes constant remodeling through the orchestrated actions of bone resorption and formation processes [1–5]. This dynamic remodeling cycle depends on the coordinated activities of osteoclasts responsible for bone degradation and osteoblasts responsible for bone matrix synthesis [3, 6]. Osteoclasts derive from hematopoietic stem cells (HSCs), while osteoblasts differentiate from multipotent mesenchymal stem/stromal cells (MSCs), which possess the capacity to differentiate into bone, fat, and cartilage [7, 8]. Dysregulated functions of osteoclasts and osteoblasts disrupt normal bone remodeling, contributing to metabolic bone disorders like osteoporosis in the aging population [9–11]. The pathogenesis of these conditions involves a complex interplay between genetic and environmental factors [12–14]. Genome-wide association studies (GWASs) have identified numerous loci associated with bone mineral density (BMD), highlighting the polygenic nature of the genetic risk for osteoporosis [14–16]. Notably, many prioritized genes implicated in BMD regulation, including

Bo Zhou, Hongwen Huang and Zhen Ding contributed equally to this work.

✉ Wenfei Jin
jinwf@sinh.ac.cn

✉ Guixing Ma
maguixing@live.com

✉ Huiling Cao
caohl@sustech.edu.cn

[1] Department of Biochemistry, School of Medicine, Southern University of Science and Technology, Guangdong Provincial Key Laboratory of Cell Microenvironment and Disease Research, Shenzhen Key Laboratory of Cell Microenvironment, Key University Laboratory of Metabolism and Health of Guangdong, Southern University of Science and Technology, Shenzhen 518055, China

[2] Department of Biology, Southern University of Science and Technology, Shenzhen 518055, China

[3] Shanghai Institute of Nutrition and Health, CAS, Shanghai 200031, China

Published online: 11 March 2025

RUNX2, ALPL, DMP1, BMP4, and *WNT4,* exhibit significant expression in osteoblasts and play crucial roles in their differentiation [15].

In the bone marrow microenvironment, MSC heterogeneity has been delineated through the expression profiling of various marker genes, including platelet-derived growth factor receptor (*Pdgrfa*, *Pdgfrb*), leptin receptor (*Lepr*), nestin (*Nes*), NG2 (*Cspg4*), paired-related homeobox protein 1 (*Prrx1*), gremlin 1 (*Grem1*), cathepsin K (*Ctsk*), zinc finger protein GLI1 (*Gli1*), fibroblast growth factor receptor 3 (*Fgfr3*), and somatostatin receptor type 2 (*Sstr2*) [17–29]. Importantly, distinct subpopulations of PDGFRα$^+$β$^+$ MSCs show regional specialization and contribute to bone formation throughout distinct development stages in both young and adult mice [27]. In adult mice, MSCs located in the bone marrow and periosteum exhibit distinguishable characteristics based on the varying expression levels of *Lepr* and *Gli1* [30]. While *Lepr*-expressing MSC (Lepr$^+$ MSC) and the descendent osteolineage cells (OLCs) have been consistently characterized, the identity of OLCs associated with other reported MSC populations remains elusive [31–33].

OLCs not only contribute to bone formation and architecture but also serve as crucial components of the bone marrow microenvironment, regulating hematopoietic homeostasis [26, 28, 34]. Dysfunctional OLCs have been linked to the development of metabolic bone diseases like osteopenia and hematopoietic disorders such as leukemia [28, 35, 36]. The differentiation of OLCs is orchestrated by Runt related transcription factor 2 (RUNX2) and a network of synergistic transcriptional regulators, including Maf, WW domain-containing transcription regulator protein 1 (WWTR1), DNA binding protein SATB2, Retinoblastoma-associated protein (RB1), zinc finger protein GLI2, and homeobox protein DLX5, MSX-2, Nkx-3.2 [4]. However, the intricate gene regulatory network governing heterogeneous OLCs with diverse origins remains elusive [37, 38]. While the application of single cell technologies such as mass cytometry and scRNA-seq has advanced our understanding in the heterogeneity of osteoblastic cell populations in adults, further efforts are required to unravel the differentiation trajectories of OLCs derived from distinct MSC populations [32, 39, 40].

In this study, we conducted an integrative analysis of 77 scRNA-seq libraries from 14 datasets, focusing on the heterogeneity of OLCs and their lineage relationships within the bone marrow microenvironment (Table S1). Through this analysis, we identified two distinct types of OLCs, namely OLC1 and OLC2, originating from distinct mesenchymal precursors. Transcriptomic profiling revealed that OLC1 and OLC2 exhibited unique molecular signatures and distinct gene regulatory networks. In addition, estimated polygenic disease association scores indicated significant associations of both OLC1 and OLC2 with the bone mineral density (BMD). Finally, we elucidated the differential impacts of OLC1 and OLC2 in aged mice, providing valuable insights into the pathogenesis of age-related osteoporosis.

Results

Single cell profiling of OLCs in adult murine bone marrow

The orchestration of osteoblast production is temporally and spatially regulated, leading to a transition from longitudinal to appositional bone remodeling following adolescence [41]. Recent lineage tracing studies have unveiled the essential roles of Lepr$^+$ MSCs and Gli1$^+$ MSCs in bone mass maintenance in adult mice [30]. To delineate osteolineages originating from these two distinct MSC populations at the single-cell level, we re-analyzed bone marrow stromal cells isolated from 3-month-old mice [42]. Initially, we assessed the expression of historically defined marker genes of MSCs across all stromal cell clusters (Fig. S1A–E). Unlike other stromal cell types such as endothelial cells and pericytes, MSCs and OLCs showed specific expression of *Pdgfra* and *Pdgfrb*. Consistent with previous findings, one subset of MSCs demonstrated high expression of characteristic markers of adult bone marrow MSCs (BM-MSCs), including *Lepr* and *Adipoq*, while the other subset of MSCs exhibited significant expression of markers associated with periosteal MSCs (P-MSCs), such as *Ctsk* and *Gli1* (Fig. S1D) [20, 24, 28, 30]. To investigate the differentiation lineages of PDGFRα$^+$β$^+$Lepr$^+$ BM-MSCs and PDGFRα$^+$β$^+$Gli1$^+$ P-MSCs in adult mice, we examined the expression profiles of osteoblastic markers (*Runx2*, *Sp7*, *Alpl*, *Bglap*), chondrocytic markers (*Acan*), and adipocytic markers (*Adipoq*) (Fig. S1F). Additionally, utilizing RNA velocity analysis, we elucidated the trajectories of OLC1 and OLC2 derived from BM-MSCs and P-MSCs, respectively (Fig. S1G).

The expression of the metaphyseal SSC marker *Sstr2* was not prominently detected in stromal cells of adult mice, indicating apparent changes in the bone marrow microenvironment following adolescence [29]. Consequently, we explored bone marrow stromal cells at postnatal day 7.5 (P7.5) (Fig. S2A). PDGFRα$^+$β$^+$ MSCs, including Sstr2$^+$ SSC, Lepr$^+$Hey1$^+$ bone marrow progenitor cells (BMPCs), Lepr$^+$Adipoq$^+$ reticular cells (RetiCs), and Ctsk$^+$Thy1$^+$ periosteal MSCs (P-MSCs) in P7.5 mice, exhibited distinct expression patterns compared to BM-MSCs and P-MSCs in adult mice (Fig. S2B). Additionally, MSCs and osteolineages in mice at P7.5 showed significant levels of proliferative activity, while both BM-MSCs and P-MSCs in adult mice were predominantly quiescent (Figs. S1E, S2C, D).

The characterization of osteo-lineage cells (OLCs) within bone marrow microenvironment remains incomplete, potentially due to a lack of integrative analysis involving large sample sizes. To further address this gap, we collected a comprehensive dataset comprising 77 scRNA-seq libraries from 14 published datasets. These datasets encompassed non-hematopoietic stromal cells from various skeletal tissues, including bone marrow, as well as Prrx1-marked potential stem cells from bone and related tissues such as iWAT (inguinal White Adipose Tissue), dermis, and muscle (Fig. S3A, B, Table S1). Following quality control procedures, we identified a total of 181, 072 non-hematopoietic stromal cells from bone marrow, along with 43, 449 Prrx1$^+$ cells from iWAT, dermis, and muscle (Fig. S3B). The specific characterization of BM-MSCs, P-MSCs, and OLCs within the bone marrow revealed distinct molecular phenotypes compared to Prrx1$^+$ cells found in inguinal white adipose tissue (iWAT), dermis, and muscle (Figs. 1A–C, S3C–E, Table S2). Specifically, we identified 17, 137 OLC1 cells and 6, 835 OLC2 cells in bone marrow microenvironment of adult mice. Taken together, our findings delineate a distinct bone marrow microenvironment conducive to bone remodeling in adult mice and, notably, identify two potential types OLCs originating from distinct precursors and occupying different anatomical locations for the first time.

OLC1 and OLC2 play distinct roles in ossification

Despite sharing common roles in ossification, OLC1 and OLC2 exhibited differential expression of functional ossification-related genes, suggesting their potentially distinct and complex roles in bone formation (Fig. 1B). To gain deeper insights into the roles of these two types of OLCs, we employed a negative binomial general linear model to thoroughly identify their uniquely expressed gene signatures. Our analysis revealed a total of 2, 430 significant genes that were differentially expressed between OLC1 and OLC2, comprising 1, 882 OLC1-specific signatures and 548 OLC2-specific signatures (Fig. 1D, Table S3). Notably, OLC1 showed significant expression of 45 osteoblast differentiation related genes, such as *Gdpd2*, *Satb2*, *Id4*, and *Wnt4*, while OLC2 highly expressed 23 osteoblast differentiation related genes, such as *Nppc*, *Ostn*, *Tnn*, and *Sfrp2*. Among them, we found *Id4* was markedly expressed in OLC1, and *Tnn* was exclusively expressed by OLC2 (Fig. 1E). Furthermore, enrichment analysis showed that OLC1 exhibited significant activity in the cell cycle, while OLC2 played an essential role in extracellular matrix (ECM) organization (Fig. 1F). Subsequently, we performed cell cycle analysis to assess G2M score and S score for individual cells within OLC1 and OLC2. Our results demonstrated limited proliferative activity in both OLC1 and OLC2, with OLC1 showing a comparatively higher proportion of cells in the S and G2M phases (Fig. 1G). Given the essential role of the ECM in bone integrity and strength, with ECM proteins being expressed across various stromal cell types in bone and marrow [43], we further investigated the roles of OLC1 and OLC2 in bone mineralization. Notably, ECM formation-related genes were found to be highly expressed in osteoblasts, chondrocytes, and OLC2 (Figs. 1H, S4A, B).

Overall, our analyses delineate the distinct signatures of OLC1 and OLC2, and provided further insights into potential functions of these two types of OLCs.

OLC1 and OLC2 originate from two distinct mesenchymal cells

To further explore their developmental trajectory, we employed partition-based graph abstraction (PAGA) and Pearson's correlation to infer connectivity and construct lineage relationships (Fig. 2A, B). Our analyses supported that BM-MSCs were the progenitors of OLC1, and P-MSCs gave rise to OLC2. Additionally, the inferred PAGA structure revealed that both OLC1 and OLC2 shared close ties with osteoblasts. Moreover, akin to osteoblasts, OLC1 and OLC2 showed high module scores indicative of osteoblast differentiation (Fig. 2C).

Moreover, we investigated the transcriptome dynamics at the single-cell level during the development of OLC1 and OLC2. To capture their developmental dynamics accurately, we modeled gene expression along the inferred pseudotime using a negative binomial general linear model. For the differentiation of BM-MSCs, we identified 5, 694 dynamically expressed genes in the lineage of OLC1 and 2, 694 dynamically expressed genes in the adipocyte lineage (Fig. 2D). Distinct transcriptional programs governed the differentiation trajectories of OLC1 and adipocyte, reflecting their distinct cellular functions during development (Fig. 2E). Specifically, genes related to RUNX2 expression and activity, such as *Runx2* and *Sp7*, were dynamically expressed in the OLC1, lineage (Fig. 2D). Regarding the differentiation of P-MSC cell, we identified 1, 630 dynamically expressed genes in the OLC1 lineage and 2, 921 genes dynamically expressed in the chondrocyte lineage (Fig. 2F). Althrough the master transcription factor *Runx2* was expressed at higher levels at the developmental terminal of chondrocytes, its downstream transcription factor *Sp7* and osteocalcin *Bglap* were significantly expressed in the OLC2 lineage. This suggests that a distinct developmental program governs the lineage of OLC2, differing from that in the OLC1 lineage. Furthermore, functional enrichment analyses revealed active

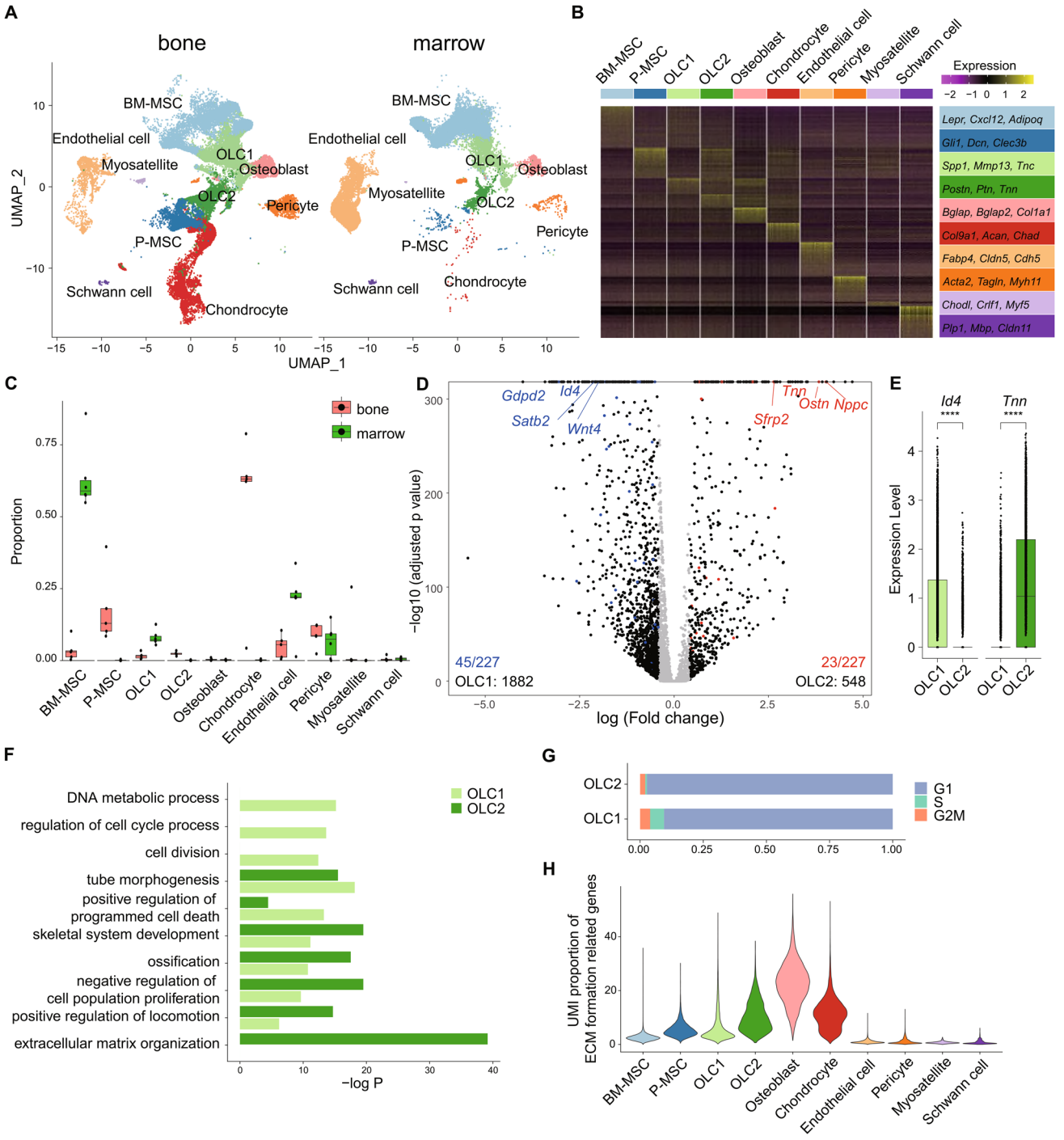

Fig. 1 Single cell analysis revealed distinct osteo-lineage cells (OLCs) in adult mice. **A** Stromal cells in bone and marrow, respectively. **B** Expression landscape of these clusters. For each cluster, 500 cells were sampled as representatives. Top six marker genes for each cluster were indicated at the right box. **C** Box plot showed the proportion of stromal cells in bone and marrow, respectively. **D** Differentially expressed genes between OLC1 and OLC2. Statistical p-values were adjusted via Bonferroni method. Genes involved in osteoblast differentiation were markers in blue (highly expressed by OLC1) and red (highly expressed by OLC2). The numbers of total signatures and osteoblast differentiation related signatures were indicated at left-bottom and right-bottom for OLC1 and OCL2, respectively. **E** Boxplot showed the expression of Id4 and Tnn in OLC1 and OLC2. **F** Functional enrichment analysis for signature genes of OLC1 and OLC2. **G** Proportion of OLC1 and OLC2 in different cell cycle phases. **H** Module score of ECM formation related genes in stromal cells

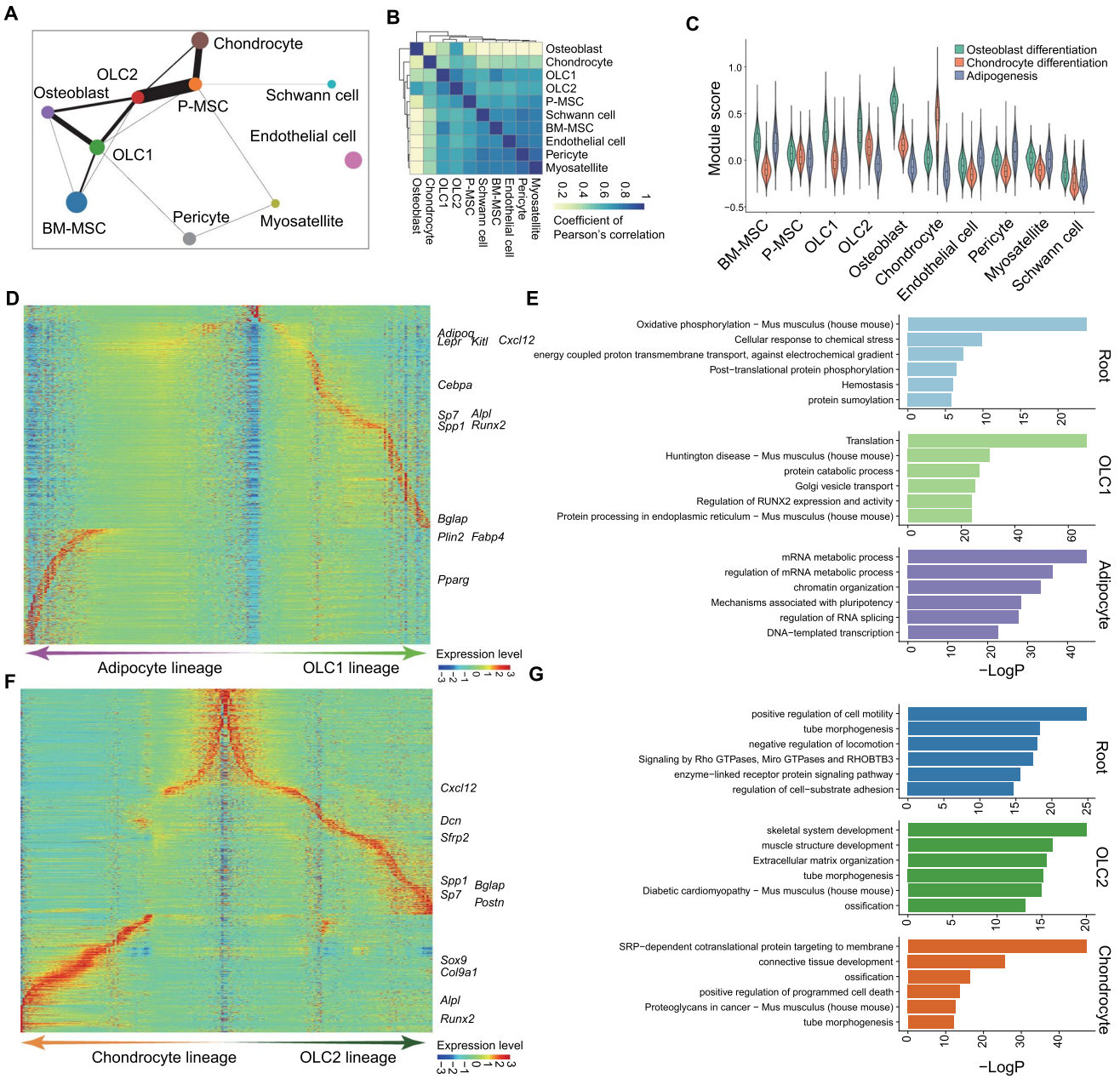

Fig. 2 Trajectory analysis indicated the differentiation lineages of OLC1 and OLC2. **A** PAGA plot of connectivity among clusters. **B** Pearson's correlation among clusters. **C** Module scores of osteoblast differentiation, chondrocyte differentiation, and adipogenesis. Corresponding gene sets of osteoblast differentiation, chondrocyte differentiation, and adipogenesis, were obtained from MSigDB. **D** Transcriptome dynamics of the differentiation of BM-MSCs. **E** Functional enrichment of the differentiation of BM-MSCs. **F** Transcriptome dynamics of the differentiation of P-MSCs. **G** Functional enrichment of the differentiation of P-MSCs

expression of ECM-related genes across the lineage of OLC2 (Fig. 2G).

Thus, our single cell analyses elucidated distinct developmental trajectories of OLC1 and OLC2, unveiling their specific transcriptome dynamics.

Gene regulatory networks in the OLC1 and OLC2

Prompted by the distinct molecular profiles of OLC1 and OLC2 lineages, we embarked on uncovering their regulatory networks of driver genes. Leveraging RNA velocity, we inferred the directional trajectories of BM-MSCs and P-MSCs differentiation, capturing the dynamics of cell states at single-cell resolution. Through this approach, we aimed to

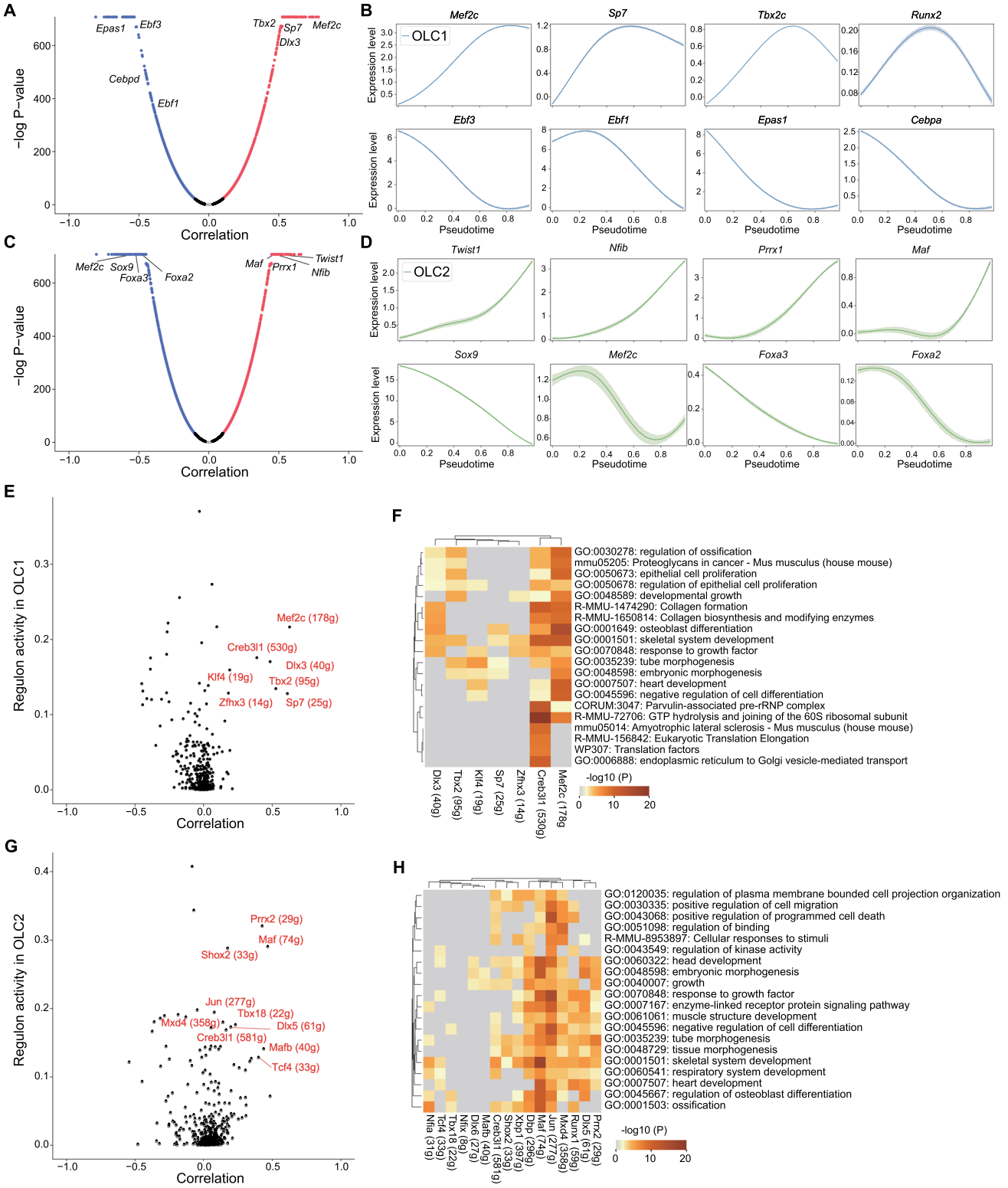

Fig. 3 The differentiation of OLC1 and OLC2 was governed by different transcription networks. **A**, **C** Correlation between the gene expression and absorption probabilities of OLC1 lineage (**A**) and OLC2 lineage (**C**). **B**, **D** Expression of potential driver genes in OLC1 lineage (**B**) and OLC2 lineage (**D**). **E**, **G** Activities of gene regulatory modules in OLC1 (**E**) and OLC2 (**G**). **F**, **H** Functional enrichment of gene regulatory modules in OLC1 (**F**) and OLC2 (**H**)

identify putative lineage-specific drivers that governing cell fate transition during differentiation (Tables S4, 5). By correlating gene expression with Markov chain-derived absorption probabilities within each lineage, we systematically uncovered the regulators potentially pivotal in the development of OLC1 and OLC2 (Fig. 3A–D). As expected, the identified drivers in the OLC1 and OLC2 lineages exhibited distinction. Notably, the expression levels of key master transcription factors governing osteoblast differentiation, including *Sp7*, *Mef2c*, *Creb3l1*, and *Satb2*, displayed significant and positive correlation with OLC1 development (Fig. 3A, B). Conversely, the upregulated expression of specific transcription factors, such as *Twist1*, *Nfib*, *Prrx1*, and *Maf*, was significantly associated with OLC2 development (Fig. 3C, D). Thus, our findings underscore the lineage-specific promotion of OLC1 and OLC2 by distinct transcription factors.

To elucidate putative direct-binding targets of the potential driver transcription factors and delineate active regulatory modules governing OLC1 and OLC2 development, we employed SCENIC to link cis-regulatory sequences to single cell gene expression [44]. Through this approach, we inferred active regulons that likely regulate the development OLC1 and OLC2. In the OLC1 lineage, seven regulatory modules were identified, driven by transcription factors *Mef2c*, *Creb3l1*, *Dlx3*, *Klf4*, *Tbx2*, *Sp7*, and *Zfhx3* (Fig. 3E). Notably, six of these regulons, including those of *Sp7*, *Mef2c*, *Creb3l1*, *Dlx3*, *Tbx2*, and *Zfhx3*, were directly involved in osteoblast differentiation and skeletal system development, while the *Klf4* regulon was associated with the regulation of growth factors and cell differentiation (Fig. 3F). Conversely, in the OLC2 lineage, we identified 16 regulons exhibiting high expression activity and robust trajectory correlation, encompassing *Prrx2*, *Maf*, *Shox2*, *Jun*, *Tbx18*, *Mxd4*, *Dlx5*, *Creb3l1*, *Mafb*, *Dlx6*, *Xbp1*, *Tcf4*, *Nfia*, *Dbp*, *Runx1*, and *Nfix* (Fig. 3G). Functional enrichment analysis demonstrated that 13 of these regulons played pivotal roles in skeletal system development, osteoblast differentiation, and ossification (Fig. 3H). Notably, our inference of single-cell regulatory networks provided further validation of the roles of driver transcription factors, as not all highly correlated transcription factors showed detectable regulon activities.

In summary, our investigation of the regulatory modules governing the lineage development of OCL1 and OLC2 indicates the presence of distinct gene regulatory networks within each lineage.

Defining OLC1 and OLC2 by surface markers

Centered on genes encoding cell membrane proteins, we identified 143 differentially expressed genes in OLC1 or OLC2, exhibiting fold changes exceeding 1.5, indicating potential specificity to these cell lineages. Through scrutinizing the expression of these genes within each cluster and filtering out shared stromal cell genes, we identified 32 candidates displaying elevated expression levels in OLC1 or OLC2 (Fig. 4A). Notably, both OLC1 and OLC2 exhibited high expression levels of *Pdgfrb* and *Ncam1* (Fig. 4A,

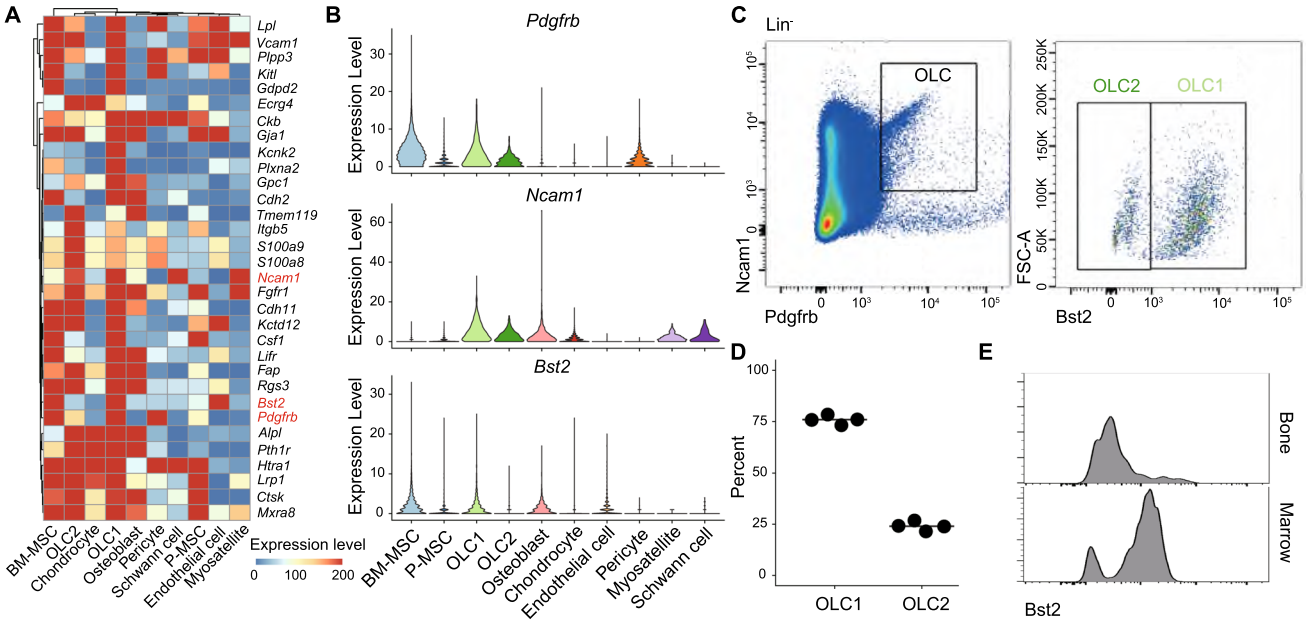

Fig. 4 Surface marker of OLC1 and OLC2. **A** Expression of candidate genes that encoded cell membrane proteins. **B** Expression of surface marker genes of OLC1 and OLC2 in stromal clusters. **C** Flow cytometry analysis of OLC1 and OLC2. **D** Relative percentage of OLC1 and OLC2 in bone marrow microenvironment of mice. **E** Expression of Bst2 in OLC from bone and marrow, respectively

B). Additionally, the expression of *Bst2* served as a distinguishing factor between OLC1 and OLC2 (Fig. 4A–C). Interestingly, Bst2$^+$ OLC1 constituted approximately 75% of Lin$^-$Pdgfrb$^+$Ncam1$^+$ OLCs in bone and marrow, while Bst2$^-$ OLC2 represented about 25% of Lin$^-$Pdgfrb$^+$Ncam1$^+$ OLCs (Fig. 4D). Furthermore, the expression levels of Bst2 in OLCs within bone and marrow displayed distinct distributions (Fig. 4E). These findings, consistent with scRNA-seq data, underscore the predominance of OLC1 in the marrow and OLC2 in bone.

OLC1 and OLC2 are associated with bone mineral density

Genome-wide association studies (GWAS) offer valuable insights into the genetic underpinnings of traits and diseases; however, the specific cell populations mediating the impacts of risk alleles remain largely unknown [45]. To evaluate the polygenic disease enrichment of OLC1 and OLC2, we employed single-cell disease relevance score (scDRS), integrating scRNA-seq data with GWAS results. Using scDRS, we assessed cell-type-disease associations within the bone marrow microenvironment across 74 diseases/traits (Fig. S5A). Notably, among these conditions, bone mineral density (BMD) exhibited a significant association with OLC1, OLC2, and osteoblasts (Fig. 5A). Conversely, BM-MSC and P-MSC populations showed limited associations with BMD. Given the close relationship between bone mineralization and mature osteocytes, we hypothesized that late developmental stages of the osteo-lineage, rather than the early stages, would exhibit a stronger association with BMD. Indeed, osteoblasts demonstrated the highest relevance score to BMD (Fig. 5B). Correspondingly, both OLC1 and OLC2 exhibited increasing BMD scores throughout their development (Fig. 5C, D).

To elucidate the genes driving the association between osteo-lineage cells (OLC1 and OLC2) and bone mineral density (BMD), we explored the correlation between gene expression and BMD score. Notably, among the BMD-relevant genes, 249 were differentially expressed OLC1, while 119 exhibited differentially expression in OLC2 (Fig. 5E). This suggests distinct functional gene profiles between OLC1 and OLC2 in their contributions to BMD (Fig. 5F). The prioritized relevant genes in OLC1 were highly involved in skeletal development, such as *Bmp1*, *Bmp3*, *Satb2*, and *Dmp1*. Conversely, the BMD-relevant genes in OLC2 were closely associated with ECM organization, featuring genes such as *Col1a1*, *Col1a2*, *Col5a1*, *Col5a2*, *Mmp2*, and *Lum*. Functional enrichment analysis further revealed that 19 OLC1-specific (*Ddr2*, *Itgav*, *Col25a1*, *Mmp16*, *Tnc*, *Sdc3*, *Dmp1*, *Ibsp*, *Spp1*, *Furin*, *Adam12*, *Bmp1*, *Mmp13*, *Plod2*, *Adamts2*, *P4hb*, *Col22a1*, *Col11a2*, *Fbn2*) and 34 OLC2-specific (*Col5a2*, *Fn1*, *Col6a3*, *Tgfb2*, *Col5a1*, *Cd44*, *Thbs1*, *Bmp2*, *Sdc4*, *Timp1*, *Ctsk*, *Col11a1*, *Col27a1*, *Col16a1*, *Col1a2*, *P4ha1*, *Col6a2*, *Col6a1*, *Dcn*, *Lum*, *Comp*, *Mmp2*, *Mmp14*, *Itga11*, *Col12a1*, *Sparc*, *Col1a1*, *Timp2*, *Sdc2*, *Lox*, *Ltbp3*, *Sh3pxd2a*, *Tnn*, *Col24a1*) BMD-relevant genes were involved in ECM organization (Fig. 5F, G). Thus, our findings underscore the pivotal roles of these lineage cells in maintaining BMD by influencing ECM organization.

Loss of OLCs contributes to age-related osteoporosis

The association between OLCs and BMD, highlighted their potential involvement in age-related osteoporosis [10]. To investigate the impact of OLC1 and OLC2, we initially examined the gene expression profiles in bone and marrow between young and aged mice. Remarkably, ECM-related genes were dramatically down-regulated in the bone of aged mice, particularly notable were the decreases in OLC2-specific ECM genes such as *Lum*, *Tnn*, *Col11a1*, and *Fn1* (Fig. 6A, B). In contrast, OLC1-specific ECM genes showed no significant changes in either bone or marrow (Fig. 6A, B).

Moreover, we assessed the expression levels of lineage driver genes for OLC1 and OLC2 in bone tissue obtained from young and aged mice. Remarkably, OCL1-associated drivers *Sp7*, *Dlx3*, and *Creb3l1*, as well as OLC2-associated drivers *Prrx2*, *Shox2*, *Dlx5*, *Nfia*, *Dlx6*, *Tcf4*, *Mxd4*, *Cre3bl1*, and *Runx1*, exhibited decreased expression in aged mice compared to their expression in young mice (Fig. 6C). This observation suggests the potential scenario wherein the reduced expression of these transcription factors in aged mice may impede the development of OLC1 and OLC2, consequently contributing to age-related osteoporosis.

This was consistently supported by immunohistochemistry (IHC) staining: Id4$^+$ OLC1s were prominently distributed in endosteum, marrow, and trabecular bone of young mice; however, they were scarcely detected in these regions in aged mice. Similarly, Tnn$^+$ OLC2s were predominantly located in the trabecular bone and periosteum of young mice, yet their presence was notably diminished in aged mice (Fig. 6D). To further validate the influence of OLC1 and OLC2 in age-related osteoporosis, we profiled single cells from bone and marrow in both young and aged mice. Intriguingly, we observed a substantial decrease in OLC1 and OLC2 populations in both bone and marrow of aged mice compared to young mice (Fig. 6E, F). These findings collectively suggest that the development of osteoblasts from OLC1 and OLC2 is dramatically suppressed in aged mice, consequently contributing to aged-related osteoporosis.

Collectively, our analyses indicate that aged mice exhibit impaired development of OLC1 and OLC2, attributable to the diminished expression of lineage-specific driver transcription factors.

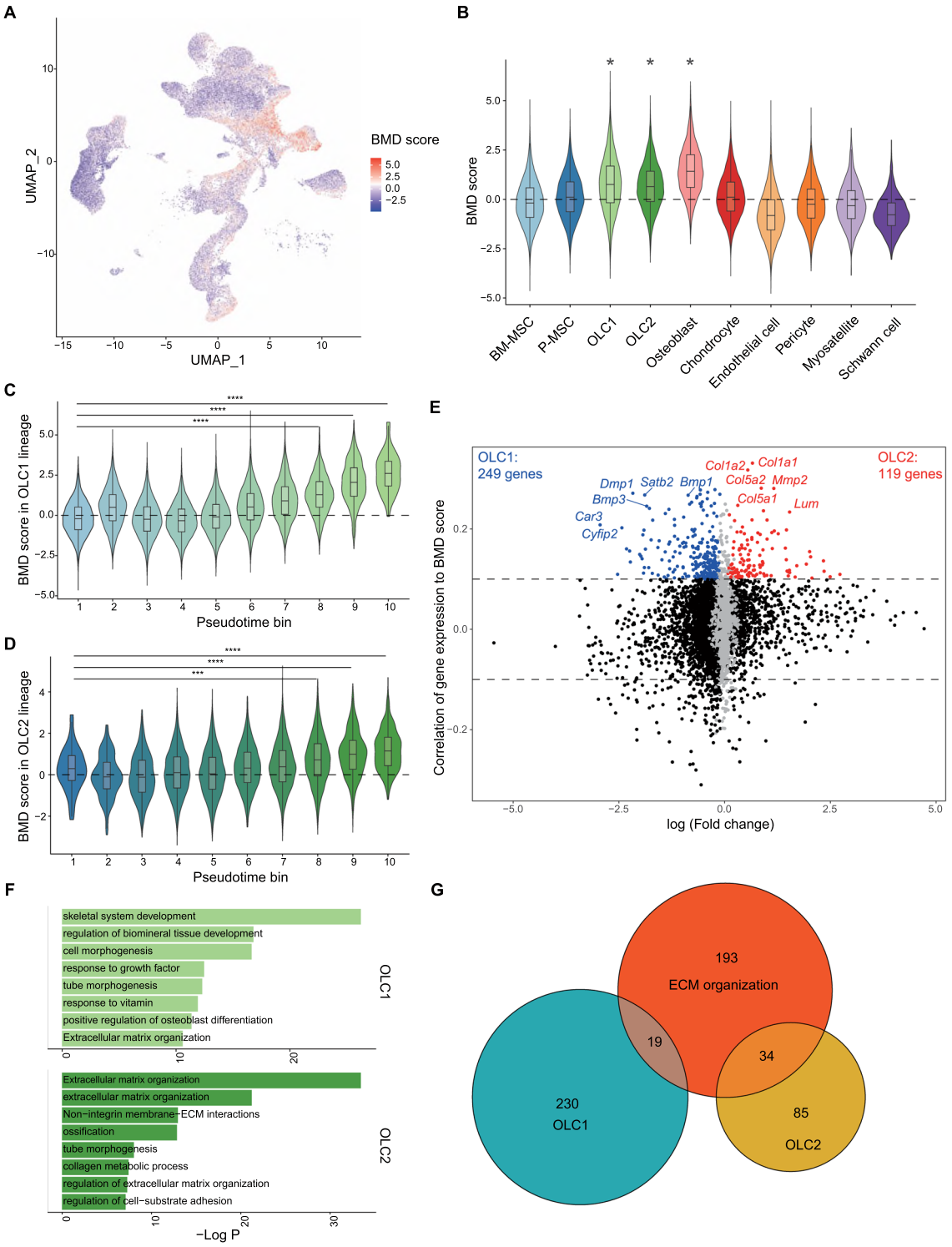

Fig. 5 Polygenic enrichment of OLC1 and OLC2. **A** Association of BMD in the bone marrow microenvironment. **B** Statistical significance of BMD association in each cluster. **C**, **D** BMD association in the OLC1 lineage (**C**) and the OLC2 lineage (**D**), cells were divided into ten bins according to their inferred pseudotime. Statistical analysis was performed with Wilcox test, and significant levels were noted above each comparison, p-value: *, < 0.05, **, < 0.01, ***, < 0.001, ****, < 0.0001. **E** Expression correlation of OLC1 and OLC2 signature genes with BMD association score, 249 OLC1 signatures with high correlation were indicated in blue, 119 OLC2 signatures with high correlation were indicated in red. **F** Functional enrichment of highly correlated signatures of OLC1 and OLC2. **G** Intersection of signature genes and ECM organization related genes

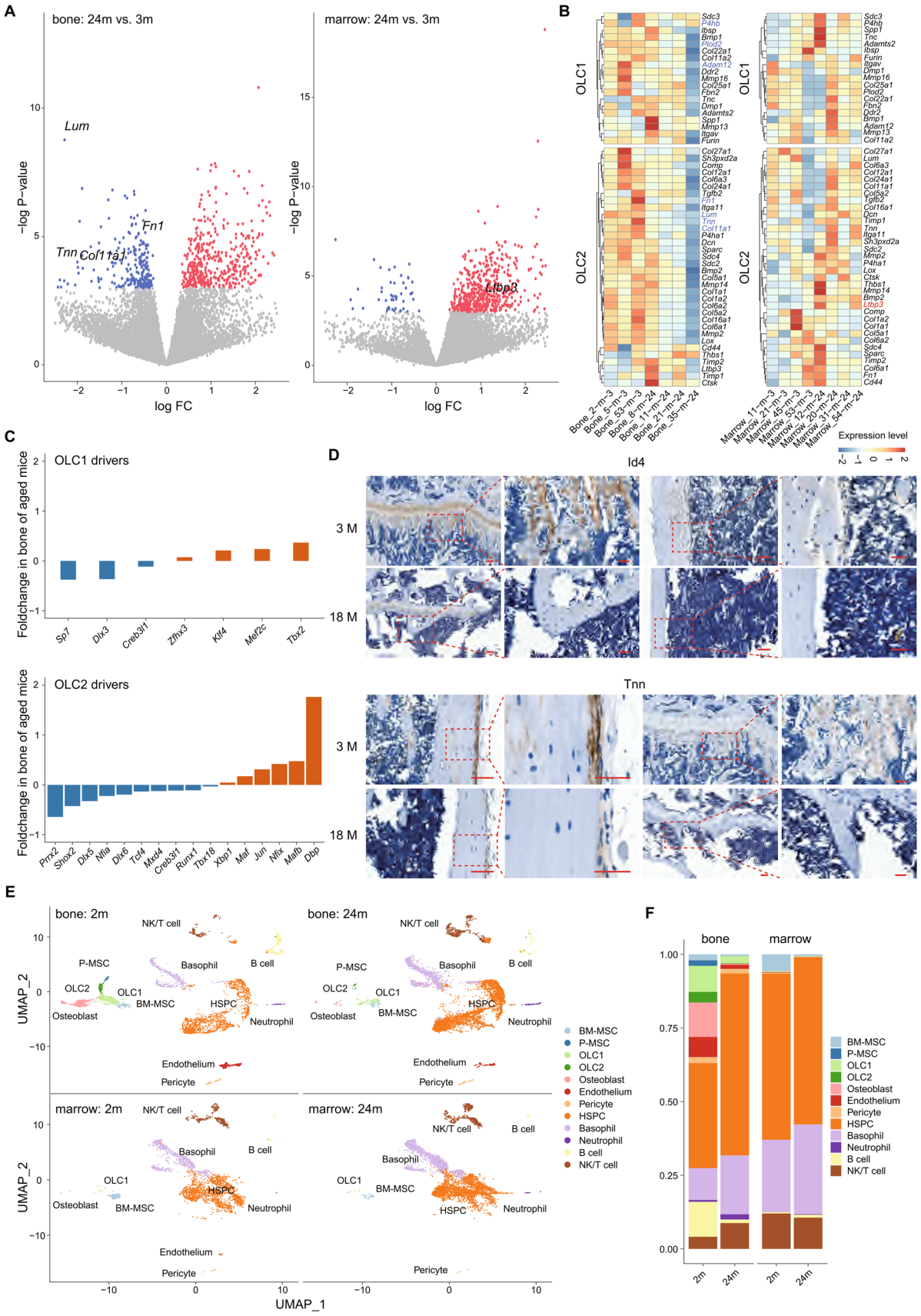
A
bone: 24m vs. 3m
marrow: 24m vs. 3m
−log P−value
log FC
Lum
Fn1
Tnn
Col11a1
Ltbp3
B
OLC1
OLC2
Bone_2−m−3
Bone_5−m−3
Bone_53−m−3
Bone_8−m−24
Bone_11−m−24
Bone_21−m−24
Bone_35−m−24
Marrow_11−m−3
Marrow_21−m−3
Marrow_45−m−3
Marrow_53−m−3
Marrow_12−m−24
Marrow_20−m−24
Marrow_31−m−24
Marrow_54−m−24
Expression level
C
OLC1 drivers
OLC2 drivers
Foldchange in bone of aged mice
Sp7
Dlx3
Creb3l1
Zfhx3
Klf4
Mef2c
Tbx2
Prrx2
Shox2
Dlx5
Nfia
Dlx6
Tcf4
Mxd4
Creb3l1
Runx1
Tbx18
Xbp1
Maf
Jun
Nfix
Mafb
Dbp
D
Id4
Tnn
3 M
18 M
E
bone: 2m
bone: 24m
marrow: 2m
marrow: 24m
UMAP_1
UMAP_2
NK/T cell
B cell
Basophil
P-MSC
OLC2
OLC1
BM-MSC
HSPC
Neutrophil
Osteoblast
Endothelium
Pericyte
F
bone
marrow
2m
24m

◂**Fig. 6** Loss of OLC1 and OLC2 in aged mice. **A** Volcano plots of differentially expressed genes in bone and marrow in aged mice, comparing with that in young mice. Statistical analysis was performed using quasi-likelihood negative binomial generalized log-linear model. **B** Expression of OLC1 and OLC2 specific ECM organization related genes in bone and marrow of young and aged mice. **C** Differential expression of OLC1 drivers and OLC2 drivers in bone and marrow of aged mice, comparing with that in young mice. **D** IHC staining of OLC1 signature Id4 and OLC2 signature Tnn in limb bone from 3 months old mice and 18 months old mice. Scale bar, zoom out: 100 μm, zoom in: 50 μm. **E** Single cell profiling of lineage depleted cells in bone and marrow of 2 months old mice and 24 months old mice. **F** Proportion of each cluster in single cell samples

Discussion

It is widely acknowledged that osteoblasts originate from various stem cell populations within the bone and marrow stromal compartment, yet the heterogeneity and transcriptome dynamics of their corresponding osteo-lineages remain incompletely understood. In this study, we conducted an integrative analysis of published datasets to comprehensively explore the bone marrow microenvironment at the single-cell level. We demonstrated the existence of two distinct OLCs, OLC1 and OLC2, characterized by their unique molecular signatures and polygenic enrichment patterns at the single-cell level. Furthermore, we elucidated their roles in age-related osteoporosis. Specifically, OLC1 exhibited high expression levels of *Spp1* and *Id4*, while OLC2 specifically expressed *Tnn* and *Ostn*. Surface protein markers such as Pdgfrb, Ncam1, and Bst2 were found to distinguish between these two cell types. Unlike OLC1 and its precursor *Lepr*$^{+}$ BM-MSCs, which were predominantly enriched in the bone marrow and trabecular bone, OLC2, characterized by the expression of *Tnn* and *Ostn*, predominantly resided in the bone periosteum. Despite their distinct characteristics, both OLC1 and OLC2 were closely associated with BMD and exhibited significant alterations in aged mice. These findings offer valuable insights into the dynamic process of bone remodeling, identifying potential cell targets for treatment of metabolic bone disorders, particularly age-related osteoporosis.

Through our integrative analysis, we have delineated two types of OLCs. OLC1, previously recognized as originating from BM-MSCs, and the newly identified OLC2, characterized by unique signatures derived from P-MSCs [32, 33]. While BM-MSCs primarily reside in the bone marrow perivascular niche, OLC1 is consistently found within the bone marrow and along the endosteal surface. In contrast, OLC2, expressing Ostn and resembling periosteal osteoblastic cells as previously characterized [46], occupies a distinct niche in the bone periosteum, setting it apart from OLC1 and another chondrogenic-origin OLC subset [32]. These two OLC types exhibit differentially expressed transcriptome, indicative of their specialized roles in ossification and bone mineralization. Notably, OLC2 emerges as a key contributor to ECM formation within the bone marrow microenvironment. Comparative analysis reveals significantly higher expression levels of numerous ECM proteins in OLC2 compared to OLC1. Specifically, genes encoding collagen subtypes (*Col3a1*, *Col5a1*, *Col6a1*, *Col6a2*, *Col6a3*, *Col7a1*, *Col8a2*. *Col12a1*), the microfibril-associated glycoprotein encoding gene *Emilin3*, lumican encoding gene *Lum*, and tenascin-N encoding gene *Tnn* are uniquely expressed in OLC2, while *Col8a1*, *Col25a1*, *Fbn2*, and *Tnc* are specifically expressed in OLC1. Our comprehensive analyses thus provide compelling evidence of the heterogeneity of OLCs within the bone marrow microenvironment.

As extensively described in previous literatures and recent single cell studies, osteoblasts arise from the osteogenic differentiation of various MSC populations and through the chondrocyte-to-osteoblast transition within the endochondral pathway [20, 25, 32, 47]. However, significant gaps remain regarding whether distinct osteo-lineage cells (OLCs) originate from different MSC populations and the transcriptional programs governing their differentiation processes. Elucidating the lineage trajectories of OLC1 and OLC2 at the single-cell level could offer critical insights into understanding the differentiation pathways of diverse MSCs. Our analysis of the transcriptome dynamics of OLC1 and OLC2 reveals both similarities and notable differences. Specifically, we observe that regulatory networks involving *Mef2c*, *Creb3l1*, *Klf4*, *Dlx3*, *Tbx2*, *Sp7*, and *Zfhx3* are prominently active in OLC1, while regulatory networks featuring *Prrx2*, *Maf*, *Shox2*, *Jun*, *Tbx18*, *Mxd4*, *Dlx5*, and *Creb3l1* are significantly expressed in OLC2. Importantly, it is evident that the differentiation trajectory of OLC2 diverges distinctly from the chondrocyte-to-osteoblast transition pathway. This is evidenced by the differential expression patterns of key markers: while *Alpl* and *Runx2* are highly expressed in hypertrophic chondrocytes during endochondral ossification, *Spp1* and *Sp7* are markedly required for OLC2 differentiation.

In conjunction with osteoblasts, both OLC1 and OCL2 exhibit pronounced relevance to BMD, a crucial predictor for osteoporosis. In addition to genes associated with osteoblast differentiation, OLC1 and OLC2 express a multitude of genes encoding ECM proteins, which play pivotal roles in BMD regulation. Notably, OLC2 demonstrates a heightened expression of 34 ECM organization-related genes significantly implicated in BMD, including *Col5a1*, *Col5a2*, *Col6a1*, *Col7a1*, and *Lum*. Thus, our findings offer compelling evidence regarding the involvement of OLC1 and OCL2 in ECM organization during bone mineralization. In aged mice, there is a noteworthy reduction in the expression levels of ECM protein-encoding genes specific to OLC2 within bone tissues, while genes related to ECM in OLC1 exhibit relatively unchanged expression profiles. This observation

suggests that OLC2 may play a particularly crucial role in age-related osteoporosis, highlighting the significance of OLC2 in the pathogenesis of metabolic bone disorders. Overall, the identification of OLC2 as a novel osteo-lineage cell type provides novel insights into the mechanisms underlying age-related bone diseases, thereby enriching our understanding of bone metabolism and offering potential avenues for therapeutic intervention.

At various life stages, osteogenesis relies on distinct osteo-lineages originating from different MSCs under both physiological homeostasis and bone regeneration scenarios [20]. Despite recent advancements shedding light on the considerable heterogeneity within MSC populations [25, 30, 39], our study identifies only two distinct types of osteo-lineages. While single-cell techniques offer unprecedented resolution for exploring the bone marrow microenvironment, they may overlook rare MSCs and osteo-lineage cells localized in specific anatomical niches [30, 32]. Consequently, it remains unclear whether additional OLCs contribute bone homeostasis in adult. Thus, future investigations should employ spatial and temporal approaches to comprehensively identify MSCs and OLCs. Nevertheless, our findings underscore the predominant roles played by these two osteo-lineages in adult bone formation. Furthermore, their specific involvement in age-related osteoporosis suggests potential therapeutic avenues targeting their development and the synthesis of ECM proteins.

Materials and methods

Single-cell data sets

We investigated the single cell studies of bone marrow in mice, which profiled stromal cells at the bone marrow microenvironment. To avoid potential unhandled exception and challenging, we only collected 10X Chromium platform generated datasets, and only samples with raw sequencing FASTQ data or processed BAM filles were used for subsequent processing. In total, we analyzed 77 samples with age ranging from 3-week-old to 16-month-old in 14 datasets (Table S1).

Data preprocessing and quality control

All samples were processed with Cell Ranger (v5.0.1) to align sequencing reads in FASTQ files to reference genome mm10 and generate feature-barcode matrices [48]. For samples with BAM files available, the BAM files were firstly converted into FASTQ files with bamtofastq (v1.2.0).

Initially, cells in raw feature-barcode matrices were accepted for un-supervised clustering analysis with Seurat pipeline [49]. In detail, there were five steps: (1) Top 3, 000 variable features were selected using variance-stabilizing transformation (vst) method; (2) The variable features were scaled and centered; (3) A PCA dimensionality reduction was then performed with the scaled variable features, and top 50 PCs were computed and stored for subsequential usage; (4) Top 30 PCs were employed to compute nearest-neighbor graph; (5) Clustering was performed with the shared nearest neighbor (SNN) modularity optimization using resolution of 2 to determine larger number of cell clusters. For filtering, clusters with mean/median UMI counts larger than 600 and mean/median detected features larger than 400 were regarded as quality-passing clusters and kept for further analysis. Remaining cells in the kept clusters were re-clustered using Seurat pipeline. Finally, clusters annotated as non-hematopoietic stromal cells based on their expressed features were used for down-streaming analysis.

Cell type annotation of clusters

Using unsupervised clustering, cells were firstly grouped into 69 clusters. Based on the expression of certain marker genes, these clusters were then merged into 10 cell types, including P-MSC (*Dcn*), BM-MSC (*Lepr*), OLC1 (*Runx2*, *Alpl*, *Spp1*), OLC2 (*Runx2*, *Alpl1*, *Postn*), Osteoblast (*Bglap*), Chondrocyte (*Sox9*, *Col9a1*, *Acan*), Endothelial (*Pecam1*, *Cdh5*), Pericyte (*Acta2*, *Myh11*), Myosatellite (*Chodl*, *Meg3*), Schwann cell (*Plp1*, *Mbp*).

Differential analysis for scRNA-seq

Generally, Wilcoxon Rank Sum test was performed to obtain marker genes in each cluster. To identify signatures for OLC1 and OLC2, we applied a negative binomial general linear model (GLM) to the transcriptome of OLC1 and OLC2 for each sample. The statistical p-value was adjusted using Bonferroni method.

Gene set functional enrichment analysis

Our target gene set was subjected to comprehensive functional enrichment analysis using Metascape, and the results were retrieved for local analyses [50]. Gene sets associated with specific Gene Ontology (GO) terms and functional categories, such as those involved in ECM organization, osteoblast differentiation, chondrocyte differentiation, and adipogenesis, were obtained from the molecular signature database (MSigDB). Subsequently, the average expression of each gene set was aggregated at the single-cell level [51].

Cell cycle analysis of scRNA-seq

To capture cell cycle phase at single cell resolution, we calculated module scores for features associated with S phase and G2M phase, respectively. Based on the inferred S score and G2M score, cells were divided into three phases: cells with G2M score higher than 0.1 but lower than S score were regarded as G2M phase, cells with S score higher than 0.1 but lower than G2M score were regarded as S phase, and cells with G2M score and S score both lower than 0.1 were taken as G1 phase.

Correlation analysis

To explore transcriptome similarity of the clusters in the bone marrow microenvironment, we firstly applied partition-based graph abstraction (PAGA) maps to estimate connectivity among clusters [52, 53]. Next, we normalized averaged gene expression for each cluster and performed Pearson's correlation analysis with genes expressed larger than 10 counts per million in any clusters.

Trajectory analysis

To identify trajectories of BM-MSCs and P-MSCs, we adopted slingshot (v2.5.2) to infer the potential cell lineages and corresponding pseudotime at single cell level [54]. To avoid potential noises due to cell cycle stages, we only included cells regarded as G1 phase for trajectory analysis. To identify transcriptome dynamics during the development of each lineage, we divided the pseudotime into ten bins, and performed GLM analysis. The significantly differentially expressed genes in each pseudotime bin were gathered together and were taken as dynamically expressed genes for the lineage.

RNA velocity analysis

By distinguishing captured mRNA molecules into spliced mRNA and unspliced mRNA with velocyto, we could estimate RNA velocity to provide cellular dynamics of developmental lineages [55]. Therefore, we applied scVelo to reconstruct the differentiation pathways [56]. Further, putative driver genes were inferred via correlating their expression against the fate absorption probability [57].

Single cell regulatory network inference

To explore the regulatory network at single cell resolution, we linked cis-regulatory sequences to the gene expression in individual cell with SCENIC [44]. In brief, co-expression modules of genes and TFs were firstly examined, targeted motif analysis was then performed to validate significant motif with correct upstream cis-regulators, and the regulons were finally identified according to their activities in individual cells.

Polygenic disease enrichment

To understand the disease association of individual cells, we applied scDRS to evaluate disease relevant scores for 74 diseases/traits with pre-constructed gene sets from genome wide association studies (GWASs) [45]. Next, we performed cell-type level analyses to determine statistical significance of disease association for each defined cell type, and conducted gene-level analyses to prioritize disease-relevant genes from expression matrices.

RNA-seq dataset

To explore transcriptome alteration for bone and marrow tissues in young and aged mice, we re-investigated bulk RNA-seq data from Tabula Muris Senis [58]. Raw counts of gene expression data of bone and marrow tissues in 3 months old young mice and 24 months old aged mice were collected for differential analysis with edgeR using quasi-likelihood negative binomial generalized log-linear model [59].

Mice

Young adult [3-month-old] and aged (24-month-old) C57BL/6 male mice were used in this study. All animal protocols were approved by the Institutional Animal Care and Use Committees of the Southern University of Science and Technology.

Cell isolation

Tibia and femur of mice were isolated, marrow was flushed out from the bone with PBS at 4 °C, while bone was digested with type II collagenase (2 mg/ml) and type IV collagenase (2 mg/ml) at 37 °C for 1 h. The cells harvested after digestion were successively filtered through 40-μm cell strainers (BD Biosciences). Lysis buffer (cat. no. C3702, Beyotime) was used for removal of red blood cells.

scRNA-seq of stromal cells in bone and marrow

After removal of hematopoietic cells using the lineage cell depletion kit (cat. no. 130-090-858; Miltenyi), we profiled stromal cells in bone and marrow from 2 months old young mice and 24 months old aged mice for scRNA-seq based on10X Genomics Chromium Single Cell 3' protocol [42].

Flow cytometry

Hematopoietic cells were excluded with the lineage cell depletion kit (Cat. No. 130-090-858; Miltenyi). Single cell suspension was blocked with 2% Fc Receptor block (eBioscience) in PBS for 15 min on ice, and stained with the following antibodies under the concentration of 1.0 μg in 100 μl volume: CD140b-APC (PDGFRb; Cat. No. 136007; Biolegend), CD56-BV605 (Ncam1; Cat. No. 748097; BD Biosciences), CD317-FITC (Bst2, Cat. No. 127007; Biolegend). Flow cytometry analysis was performed with a FACSAria instrument (BD Biosciences), and FACS data was analyzed with Flowjo (v10.8.1).

Immunohistochemistry (IHC)

IHC was performed as previously reported [60]. In brief, five-micrometer-thick sections from formalin-fixed and paraffin-embedded tissues were incubated with primary antibodies at 4 °C overnight, followed by incubation with secondary antibodies. Chromogen development was determined by DAB Kit (Vectorlabs, SK-4100). A Multifunctional digital pathology scanner (Aperio VERSA 8) was used to scan the total area of each slide.

Statistical analysis

Wilcoxon Rank Sum test was used for differential analyses for scRNA-seq. And all gene-level p-values were adjusted with Bonferroni method.

Supplementary Information The online version contains supplementary material available at https://doi.org/10.1007/s00018-025-05597-w.

Acknowledgements We acknowledge the assistance of Core Research Facilities of Southern University of Science and Technology.

Author contributions Conceptualization: B.Z., W.J., G.M., H.C. Methodology: B.Z., K.L., Y.C., W.J., G.M., H.C. Investigation: B.Z., H.M., Z.D., G.M., K.L., Y.C., Y.H., W.P., W.T., L.C. Supervision: W.J., G.M., H.C. Writing—original draft: B.Z., G.M., H.C. Writing—review & editing: B.Z., G.M., H.C.

Funding This work was supported, in part, by the National Key Research and Development Program of China Grants (2024YFA0919203), the National Natura Science Foundation of China Grants (82372476 and 82350710800), Guangdong Provincial Science and Technology Innovation Council Grant (2017B030301018), China Postdoctoral Science Fund (2023M741541).

Data and availability of materials All data related to this study are available within the Article or the Supplementary Materials and all data are available from the corresponding authors upon reasonable request.

Declaration

Conflict of interest The authors declare no conflict of interests.

Ethical approval All animal experiments were approved by the Institutional Animal Care and Use Committee (IACUC) of Southern University of Science and Technology. We affirm that we have all relevant ethical regulations for animal testing and research in this study.

References

1. Kollet O, Dar A, Shivtiel S, Kalinkovich A, Lapid K, Sztainberg Y et al (2006) Osteoclasts degrade endosteal components and promote mobilization of hematopoietic progenitor cells. Nat Med 12(6):657–664
2. Walsh MC, Kim N, Kadono Y, Rho J, Lee SY, Lorenzo J, Choi Y (2006) Osteoimmunology: interplay between the immune system and bone metabolism. Annu Rev Immunol 24:33–63
3. Crockett JC, Rogers MJ, Coxon FP, Hocking LJ, Helfrich MH (2011) Bone remodelling at a glance. J Cell Sci 124(Pt 7):991–998
4. Long F (2011) Building strong bones: molecular regulation of the osteoblast lineage. Nat Rev Mol Cell Biol 13(1):27–38
5. Burr DB, Gallant MA (2012) Bone remodelling in osteoarthritis. Nat Rev Rheumatol 8(11):665–673
6. Salhotra A, Shah HN, Levi B, Longaker MT (2020) Mechanisms of bone development and repair. Nat Rev Mol Cell Biol 21(11):696–711
7. Boyle WJ, Simonet WS, Lacey DL (2003) Osteoclast differentiation and activation. Nature 423(6937):337–342
8. Kfoury Y, Scadden DT (2015) Mesenchymal cell contributions to the stem cell niche. Cell Stem Cell 16(3):239–253
9. Khosla S, Riggs BL (2005) Pathophysiology of age-related bone loss and osteoporosis. Endocrinol Metab Clin North Am 34(4):1015–1030
10. Feng X, McDonald JM (2011) Disorders of bone remodeling. Annu Rev Pathol 6:121–145
11. Bolamperti S, Villa I, Rubinacci A (2022) Bone remodeling: an operational process ensuring survival and bone mechanical competence. Bone Res 10(1):48
12. Singer FR (2015) Paget's disease of bone-genetic and environmental factors. Nat Rev Endocrinol 11(11):662–671
13. Karasik D, Rivadeneira F, Johnson ML (2016) The genetics of bone mass and susceptibility to bone diseases. Nat Rev Rheumatol 12(6):323–334
14. Kim SK (2018) Identification of 613 new loci associated with heel bone mineral density and a polygenic risk score for bone mineral density, osteoporosis and fracture. PLoS ONE 13(7):e0200785

15. Kemp JP, Morris JA, Medina-Gomez C, Forgetta V, Warrington NM, Youlten SE et al (2017) Identification of 153 new loci associated with heel bone mineral density and functional involvement of GPC6 in osteoporosis. Nat Genet 49(10):1468–1475
16. Wang H, Zhang F, Zeng J, Wu Y, Kemper KE, Xue A et al (2019) Genotype-by-environment interactions inferred from genetic effects on phenotypic variability in the UK Biobank. Sci Adv 5(8):eaaw3538
17. Mendez-Ferrer S, Michurina TV, Ferraro F, Mazloom AR, Macarthur BD, Lira SA et al (2010) Mesenchymal and haematopoietic stem cells form a unique bone marrow niche. Nature 466(7308):829–834
18. Ding L, Saunders TL, Enikolopov G, Morrison SJ (2012) Endothelial and perivascular cells maintain haematopoietic stem cells. Nature 481(7382):457–462
19. Kunisaki Y, Bruns I, Scheiermann C, Ahmed J, Pinho S, Zhang D et al (2013) Arteriolar niches maintain haematopoietic stem cell quiescence. Nature 502(7473):637–643
20. Zhou BO, Yue R, Murphy MM, Peyer JG, Morrison SJ (2014) Leptin-receptor-expressing mesenchymal stromal cells represent the main source of bone formed by adult bone marrow. Cell Stem Cell 15(2):154–168
21. Chan CK, Seo EY, Chen JY, Lo D, McArdle A, Sinha R et al (2015) Identification and specification of the mouse skeletal stem cell. Cell 160(1–2):285–298
22. Worthley DL, Churchill M, Compton JT, Tailor Y, Rao M, Si Y et al (2015) Gremlin 1 identifies a skeletal stem cell with bone, cartilage, and reticular stromal potential. Cell 160(1–2):269–284
23. de Lageneste OD, Julien A, Abou-Khalil R, Frangi G, Carvalho C, Cagnard N et al (2018) Periosteum contains skeletal stem cells with high bone regenerative potential controlled by Periostin. Nat Commun 9:773
24. Debnath S, Yallowitz AR, McCormick J, Lalani S, Zhang T, Xu R et al (2018) Discovery of a periosteal stem cell mediating intramembranous bone formation. Nature 562(7725):133–139
25. Liu H, Li P, Zhang S, Xiang J, Yang R, Liu J et al (2022) Prrx1 marks stem cells for bone, white adipose tissue and dermis in adult mice. Nat Genet 54(12):1946–1958
26. Matsushita Y, Liu J, Chu AKY, Tsutsumi-Arai C, Nagata M, Arai Y et al (2023) Bone marrow endosteal stem cells dictate active osteogenesis and aggressive tumorigenesis. Nat Commun 14(1):2383
27. Sivaraj KK, Jeong HW, Dharmalingam B, Zeuschner D, Adams S, Potente M, Adams RH (2021) Regional specialization and fate specification of bone stromal cells in skeletal development. Cell Rep 36(2):109352
28. Shi Y, He GX, Lee WC, McKenzie JA, Silva MJ, Long FX (2017) Gli1 identifies osteogenic progenitors for bone formation and fracture repair. Nat Commun 8:773
29. Yang G, He Q, Guo X, Li RY, Lin J, Lang Y et al (2024) Identification of the metaphyseal skeletal stem cell building trabecular bone. Sci Adv 10(8):eadl2238
30. Jeffery EC, Mann TLA, Pool JA, Zhao Z, Morrison SJ (2022) Bone marrow and periosteal skeletal stem/progenitor cells make distinct contributions to bone maintenance and repair. Cell Stem Cell 29(11):1547–1561
31. Ono N, Ono W, Nagasawa T, Kronenberg HM (2014) A subset of chondrogenic cells provides early mesenchymal progenitors in growing bones. Nat Cell Biol 16(12):1157–1167
32. Baryawno N, Przybylski D, Kowalczyk MS, Kfoury Y, Severe N, Gustafsson K et al (2019) A cellular taxonomy of the bone marrow stroma in homeostasis and leukemia. Cell 177(7):1915–32.e16
33. Wolock SL, Krishnan I, Tenen DE, Matkins V, Camacho V, Patel S et al (2019) Mapping distinct bone marrow niche populations and their differentiation paths. Cell Rep 28(2):302–311
34. Yu VWC, Lymperi S, Oki T, Jones A, Swiatek P, Vasic R et al (2016) Distinctive mesenchymal-parenchymal cell pairings govern B cell differentiation in the bone marrow. Stem Cell Rep 7(2):220–235
35. Raaijmakers MHGP, Mukherjee S, Guo SQ, Zhang SY, Kobayashi T, Schoonmaker JA et al (2010) Bone progenitor dysfunction induces myelodysplasia and secondary leukaemia. Nature 464(7290):852-U58
36. Wu XH, Qu MH, Gong WY, Zhou CL, Lai YM, Xiao GZ (2022) Kindlin-2 deletion in osteoprogenitors causes severe chondrodysplasia and low-turnover osteopenia in mice. J Orthop Transl 32:41–8
37. Mizoguchi T, Ono N (2021) The diverse origin of bone-forming osteoblasts. J Bone Miner Res 36(8):1432–47
38. Yoshioka H, Okita S, Nakano M, Minamizaki T, Nubukiyo A, Sotomaru Y et al (2021) Single-cell RNA-sequencing reveals the breadth of osteoblast heterogeneity. JBMR Plus 5(6):e10496
39. Tikhonova AN, Dolgalev I, Hu H, Sivaraj KK, Hoxha E, Cuesta-Dominguez A et al (2019) The bone marrow microenvironment at single-cell resolution. Nature 569(7755):222–228
40. Doolittle ML, Saul D, Kaur J, Rowsey JL, Vos SJ, Pavelko KD et al (2023) Multiparametric senescent cell phenotyping reveals targets of senolytic therapy in the aged murine skeleton. Nat Commun 14(1):4587
41. Shu HS, Liu YL, Tang XT, Zhang XS, Zhou B, Zou W, Zhou BO (2021) Tracing the skeletal progenitor transition during postnatal bone formation. Cell Stem Cell 28(12):2122–36 e3
42. Fu X, Zhou B, Yan Q, Tao C, Qin L, Wu X et al (2020) Kindlin-2 regulates skeletal homeostasis by modulating PTH1R in mice. Signal Transduct Target Ther 5(1):297
43. Fontcuberta-Rigo M, Nakamura M, Puigbò P (2023) Phylobone: a comprehensive database of bone extracellular matrix proteins in human and model organisms. Bone Res 11(1):44
44. Aibar S, Gonzalez-Blas CB, Moerman T, Huynh-Thu VA, Imrichova H, Hulselmans G et al (2017) SCENIC: single-cell regulatory network inference and clustering. Nat Methods 14(11):1083–6
45. Zhang MJY, Hou KC, Dey KK, Sakaue S, Jagadeesh KA, Weinand K et al (2022) Polygenic enrichment distinguishes disease associations of individual cells in single-cell RNA-seq data. Nat Genet 54(10):1572
46. Watanabe-Takano H, Ochi H, Chiba A, Matsuo A, Kanai Y, Fukuhara S et al (2021) Mechanical load regulates bone growth via periosteal Osteocrin. Cell Rep 36(2):109380
47. Yang L, Tsang KY, Tang HC, Chan D, Cheah KSE (2014) Hypertrophic chondrocytes can become osteoblasts and osteocytes in endochondral bone formation. Proc Natl Acad Sci U S A 111(33):12097–102
48. Zheng GX, Terry JM, Belgrader P, Ryvkin P, Bent ZW, Wilson R et al (2017) Massively parallel digital transcriptional profiling of single cells. Nat Commun 8:14049
49. Butler A, Hoffman P, Smibert P, Papalexi E, Satija R (2018) Integrating single-cell transcriptomic data across different conditions, technologies, and species. Nat Biotechnol 36(5):411–20
50. Zhou Y, Zhou B, Pache L, Chang M, Khodabakhshi AH, Tanaseichuk O et al (2019) Metascape provides a biologist-oriented resource for the analysis of systems-level datasets. Nat Commun 10(1):1523
51. Castanza AS, Recla JM, Eby D, Thorvaldsdóttir H, Bult CJ, Mesirov JP (2023) Extending support for mouse data in the Molecular Signatures Database (MSigDB). Nat Methods 20:1619
52. Wolf FA, Angerer P, Theis FJ (2018) SCANPY: large-scale single-cell gene expression data analysis. Genome Biol 19(1):15
53. Wolf FA, Hamey FK, Plass M, Solana J, Dahlin JS, Gottgens B et al (2019) PAGA: graph abstraction reconciles clustering

with trajectory inference through a topology preserving map of single cells. Genome Biol 20(1):59
54. Street K, Risso D, Fletcher RB, Das D, Ngai J, Yosef N et al (2018) Slingshot: cell lineage and pseudotime inference for single-cell transcriptomics. BMC Genomics 19(1):477
55. La Manno G, Soldatov R, Zeisel A, Braun E, Hochgerner H, Petukhov V et al (2018) RNA velocity of single cells. Nature 560(7719):494–8
56. Bergen V, Lange M, Peidli S, Wolf FA, Theis FJ (2020) Generalizing RNA velocity to transient cell states through dynamical modeling. Nat Biotechnol 38:1408
57. Lange M, Bergen V, Klein M, Setty M, Reuter B, Bakhti M et al (2022) Cell Rank for directed single-cell fate mapping. Nat Methods 19(2):159–70
58. Schaum N, Lehallier B, Hahn O, Palovics R, Hosseinzadeh S, Lee SE et al (2020) Ageing hallmarks exhibit organ-specific temporal signatures. Nature 583(7817):596
59. Robinson MD, McCarthy DJ, Smyth GK (2010) edgeR: a Bioconductor package for differential expression analysis of digital gene expression data. Bioinformatics 26(1):139–40
60. Hou X, Chen Y, Zhou B, Tang W, Ding Z, Chen L et al (2023) Talin-1 inhibits Smurf1-mediated Stat3 degradation to modulate β-cell proliferation and mass in mice. Cell Death Dis 14(10):709